J|A|C|S ARTICLES

Published on Web 07/22/2010

Surface Charge of Electrosprayed Water Nanodroplets: A Molecular Dynamics Study

Elias Ahadi and Lars Konermann*

Department of Chemistry, The University of Western Ontario, London, Ontario N6A 5B7, Canada

Received May 15, 2010; E-mail: konerman@uwo.ca

Abstract: Aqueous nanodroplets that contain excess charge carriers play a central role during the electrospray ionization (ESI) process. An interesting question concerns the charge carrier location in these systems. In analogy to the behavior of metallic conductors, it is often assumed that excess ions are confined to a thin layer on the droplet surface. However, it is unclear whether simple electrostatic arguments adequately reflect the nanodroplet behavior. In particular, most ions tend to be heavily solvated, such that placing them at the liquid/vapor interface would be enthalpically unfavorable. In this work, molecular dynamics simulations are used to study the properties of Na^+-containing water nanodroplets close to the Rayleigh limit. In apparent violation of the surface charge paradigm, it is found that the ions reside inside the droplet. Electrostatic mapping reveals that all of the excess charge is nonetheless located on the surface. This conundrum is resolved by considering the effects of orientational water polarization. Buried Na^+ ions cause large-scale dipole ordering that extends all the way to the droplet periphery. Here, the positive ends of water dipoles preferentially point into the vapor phase. These half-dipoles in the outermost droplet layers assume the role of surface charge, while solvation effectively neutralizes Na^+ ions in the interior. Overall, our data reaffirm the validity of the surface charge paradigm for ESI nanodroplets, albeit with the caveat that this paradigm does NOT require charge carriers (ions) to be located at the water/vapor interface.

Introduction

Electrospray ionization (ESI) mass spectrometry (MS)[1] is an analytical method that has found scientific and commercial applications in many areas.[2−4] The ESI process commences when a flow of analyte solution (e.g., the eluent from a chromatographic column) is passed through a metal capillary to which a positive potential of several kilovolts has been applied.[5] ESI-MS studies often employ mixtures of water and organic cosolvents, but purely aqueous solutions may be used as well.[6] The capillary outlet is separated from the ion sampling interface of the mass spectrometer by an atmospheric pressure gap. The interface is held at a potential close to ground, and it acts as counterelectrode. The ensuing electric field leads to electrophoretic charge separation within the solution at the capillary tip. The liquid emanating from the capillary is drawn out into a Taylor cone that emits positively charged droplets. Excess charge on these droplets may be due to various cationic species, including Na^+, NH_4^+, and H^+.[7−9] The described scenario applies to the commonly used positive-ion ESI mode. It is also possible to produce droplets carrying excess anions, by applying a negative potential to the metal capillary.[10]

The size of the droplets emitted from the Taylor cone is in the micrometer range. Subsequent solvent evaporation increases the charge density until the droplets become unstable at the Rayleigh limit where the net charge Q_R is given by[5,11]

$$Q_R = 8\pi(\varepsilon_0\gamma R^3)^{1/2} \quad (1)$$

where ε_0 is the vacuum permittivity, γ is the surface tension, and R is the droplet radius. Jet emission at the Rayleigh limit leads to the formation of smaller progeny droplets.[12−15] Following several evaporation/fission cycles, the process ultimately yields nanometer-sized droplets that can release gas-phase analyte ions.[5] For ESI experiments that employ organic/aqueous mixtures, the water percentage of these nanodroplets can be greatly enhanced as a result of differential vapor pressures.[16,17] The past few years have witnessed considerable progress in the general understanding of the ESI mechanism.[5,7,18−20] However,

(1) Fenn, J. B.; Mann, M.; Meng, C. K.; Wong, S. F.; Whitehouse, C. M. *Science* **1989**, *246*, 64–71.
(2) Griffiths, *J. Anal. Chem.* **2008**, *80*, 5678–5683.
(3) Hofstadler, S. A.; Sannes-Lowery, K. A. *Nat. Rev. Drug Discovery* **2006**, *5*, 585–595.
(4) Kaltashov, I. A.; Bobst, C. E.; Abzalimov, R. R.; Berkowitz, S. A.; Houde, D. *J. Am. Soc. Mass Spectrom.* **2010**, *21*, 323–337.
(5) Kebarle, P.; Verkerk, U. H. *Mass Spectrom. Rev.* **2009**, *28*, 898–917.
(6) Benesch, J. L. P.; Ruotolo, B. T.; Simmons, D. A.; Robinson, C. V. *Chem. Rev.* **2007**, *107*, 3544–3567.
(7) Van Berkel, G. J.; Kertesz, V. *Anal. Chem.* **2007**, *79*, 5511–5520.
(8) Verkerk, U. H.; Kebarle, P. *J. Am. Soc. Mass Spectrom.* **2005**, *16*, 1325–1341.
(9) Felitsyn, N.; Peschke, M.; Kebarle, P. *Int. J. Mass Spectrom. Ion Processes* **2002**, *219*, 39–62.
(10) Loo, J. A.; Loo, R. R. O.; Light, K. J.; Edmonds, C. G.; Smith, R. D. *Anal. Chem.* **1992**, *64*, 81–88.
(11) Rayleigh, L. *Philos. Mag.* **1882**, *14*, 184–186.
(12) Gomez, A.; Tang, K. *Phys. Fluids* **1994**, *6*, 404–414.
(13) Duft, D.; Achtzehn, T.; Muller, R.; Huber, B. A.; Leisner, T. *Nature* **2003**, *421*, 128.
(14) Konermann, L. *J. Am. Soc. Mass Spectrom.* **2009**, *20*, 496–506.
(15) Marginean, I.; Znamenskiy, V.; Vertes, A. *J. Phys. Chem. B* **2006**, *110*, 6397–6404.
(16) Wang, R.; Zenobi, R. *J. Am. Soc. Mass Spectrom.* **2010**, *21*, 378–385.
(17) Zhou, S.; Cook, K. D. *Anal. Chem.* **2000**, *72*, 963–969.
(18) Kaltashov, I. A.; Mohimen, A. *Anal. Chem.* **2005**, *77*, 5370–5379.

10.1021/ja1041989

the final step that generates free analyte ions from highly charged nanodroplets remains enigmatic.[21] In addition to the classical theories of charged residue mechanism[22−24] versus ion evaporation model,[25,26] alternative scenarios have been proposed.[27]

A basic assumption of currently existing ESI models is that excess charge carriers are confined to a thin layer at the droplet surface.[5,24,25,27−30] This view originates from simple electrostatic arguments for a conducting sphere, where a quasi-continuum description is used for both solvent and charge.[31] However, it remains an open question whether these arguments are applicable to charged nanodroplets. One concern is that placing charge carriers at a liquid/vapor interface should result in the loss of enthalpically favorable solvation interactions. Also, the Onsager−Samaras[32] image charge formalism predicts that ions will be repelled from a dielectric interface such as the one between an aqueous solution and the vapor phase [κ_e(water) ≈ 80, κ_e(vapor) ≈ 1].[33−35] Indeed, molecular dynamics (MD) simulations[36−41] and surface tension measurements[42] reveal a depletion of small, nonpolarizable ions (such as Na^+, K^+, and F^-) at the surface of planar water slabs. In contrast, anions with large electronic polarizabilities such as Br^- and I^- appear to accumulate at the surface.[34,38] Recent computational studies predict a high surface affinity also for solvated protons,[43] although experimental work does not necessarily support this notion.[41] Most previous investigations on the behavior of ions at interfaces have focused on planar systems carrying zero excess charge. Hence, the implications of those studies for ESI nanodroplets are not immediately clear.[33] A related issue that is not widely discussed in the ESI literature concerns the occurrence of solvent ordering in the droplet periphery,[44] a factor that could have implications for analyte interactions with the surface.[19,45] Sum frequency generation (SFG) spectroscopy and MD studies have shown that the properties of planar water/vapor interfaces resemble those at a hydrophobic surface.[41,46−49]

Overall, it appears that the widely used model of highly charged nanodroplets as homogeneous spheres with a thin layer of surface charge[5,24,25,27−30] needs to be carefully scrutinized, if improved models of the final ESI steps are to be developed. Experimental investigations on the behavior of nanodroplets are not straightforward, but recent MD studies have begun to reveal interesting aspects of their properties.[15,50−55]

An earlier study from our laboratory[44] employed the SPC/E water model[56] for MD simulations on water droplets close to the Rayleigh limit. The SPC/E framework was extended to include excess protons as highly mobile charge carriers. Protons were found to reside at radial positions around $^2/_3R$, that is, not at the surface. The observed behavior was tentatively attributed to an interplay of Coulomb repulsion, solvation effects,[36] surface water ordering,[41,47−49] and Onsager−Samaras depletion.[32] However, solvated protons likely exhibit the most complex behavior of all ESI charge carriers. Therefore the predictive power of simple H^+ models is limited.[44] In particular, these models cannot adequately account for Zundel or Eigen-type solvation,[57] Grotthus migration,[58,59] and possible amphiphilic effects that might enhance surface affinity.[43] Hence, many fundamental aspects of ESI nanodroplets will be more readily accessible by focusing on charge carriers other than protons.

This work employs MD simulations for exploring the properties of nanometer-sized water droplets that are charged with atomic ions. We specifically focus on the behavior of Na^+. This choice is motivated by the fact that Na^+-containing droplets play an important role for mechanistic investigations on the ESI process.[5,25,50] Moreover, electronic polarization effects have been shown to be negligible for the surface affinity of Na^+, a fact that greatly simplifies the data interpretation of this work.[36−42,55] We find that all Na^+ ions adopt positions in the nanodroplet interior. It is tempting to rush to the conclusion that this behavior violates the commonly accepted surface charge paradigm. However, closer inspection reveals an interesting mechanism that amounts to dipole-mediated charge transfer from the droplet interior to the surface. As a result, excess charge *is* located on the surface the droplets, as expected on the basis of simple electrostatic arguments. At the same time, the actual charge carriers (ions) are *not* located on the surface but buried in the interior where they are extensively solvated. This

(19) Cech, N. B.; Enke, C. G. *Mass Spectrom. Rev.* **2001**, *20*, 362–387.
(20) Cole, R. B. *Electrospray Ionization Mass Spectrometry*; John Wiley & Sons, Inc.: New York, 1997.
(21) Wang, G.; Cole, R. B. *Anal. Chim. Acta* **2000**, *406*, 53–65.
(22) Dole, M.; Mack, L. L.; Hines, R. L.; Mobley, R. C.; Ferguson, L. D.; Alice, M. B. *J. Chem. Phys.* **1968**, *49*, 2240–2249.
(23) de la Mora, F. J. *Anal. Chim. Acta* **2000**, *406*, 93–104.
(24) Iavarone, A. T.; Williams, E. R. *J. Am. Chem. Soc.* **2003**, *125*, 2319–2327.
(25) Iribarne, J. V.; Thomson, B. A. *J. Chem. Phys.* **1975**, *64*, 2287–2294.
(26) Nguyen, S.; Fenn, J. B. *Proc. Natl. Acad. Sci. U.S.A.* **2007**, *104*, 1111–1117.
(27) Hogan, C. J.; Carroll, J. A.; Rohrs, H. W.; Biswas, P.; Gross, M. L. *Anal. Chem.* **2009**, *81*, 369–377.
(28) Fenn, J. B.; Rosell, J.; Meng, C. K. *J. Am. Soc. Mass Spectrom.* **1997**, *8*, 1147–1157.
(29) Fenn, J. B. *J. Am. Soc. Mass Spectrom.* **1993**, *4*, 524–535.
(30) Bruins, A. P. *J. Chromatogr. A* **1998**, *794*, 345–357.
(31) Halliday, D.; Resnick, R.; Krane, K. S. *Physics*, 4th ed.; Wiley: New York, 1992.
(32) Onsager, L.; Samaras, N. N. T. *J. Chem. Phys.* **1934**, *2*, 528–536.
(33) Messina, R. *J. Phys.: Condens. Matter* **2009**, *21*, 1–18.
(34) Jungwirth, P.; Tobias, D. J. *J. Phys. Chem. B* **2002**, *106*, 6361–6373.
(35) Chang, T.-M.; Dang, L. X. *Chem. Rev.* **2006**, *106*, 1305–1322.
(36) Benjamin, I. *J. Chem. Phys.* **1991**, *95*, 3698–3709.
(37) Jungwirth, P.; Tobias, D. J. *J. Phys. Chem. B* **2001**, *105*, 10468–10472.
(38) Wick, C. D.; Dang, L. X. *Chem. Phys. Lett.* **2008**, *458*, 1–5.
(39) Knipping, E. M.; Lakin, M. J.; Foster, K. L.; Jungwirth, P.; Tobias, D. J.; Gerber, R. B.; Dabdub, D.; Finlayson-Pitts, B. J. *Science* **2000**, *288*, 301–306.
(40) Burnham, C. J.; Petersen, M. K.; Day, T. J. F.; Iyengar, S. S.; Voth, G. A. *J. Chem. Phys.* **2006**, *124*, 024327.
(41) Tian, C. S.; Shen, Y. R. *Proc. Natl. Acad. Sci. U.S.A.* **2009**, *106*, 15148–15153.
(42) Petersen, P. B.; Saykally, R. J. *Chem. Phys. Lett.* **2008**, *458*, 255–261.
(43) Iuchi, S.; Chen, H.; Paesani, F.; Voth, G. A. *J. Phys. Chem. B* **2009**, *113*, 4017–4030.
(44) Ahadi, E.; Konermann, L. *J. Phys. Chem. B* **2009**, *113*, 7071–7080.
(45) Kuprowski, M. C.; Konermann, L. *Anal. Chem.* **2007**, *79*, 2499–2506.
(46) Chandler, D. *Nature* **2005**, *437*, 640–647.
(47) Du, Q.; Freysz, E.; Shen, Y. R. *Science* **1994**, *264*, 826–828.
(48) Trudeau, T. G.; Jena, K. C.; Hore, D. K. *J. Phys. Chem. C* **2009**, *113*, 20002–20008.
(49) Moore, F. G.; Richmond, G. L. *Acc. Chem. Res.* **2008**, *41*, 739–748.
(50) Znamenskiy, V.; Marginean, I.; Vertes, A. *J. Phys. Chem. A* **2003**, *107*, 7406–7412.
(51) Consta, S.; Mainer, K. R.; Novak, W. *J. Chem. Phys.* **2003**, *119*, 10125–10132.
(52) Ichiki, K.; Consta, S. *J. Phys. Chem. B* **2006**, *110*, 19168–19175.
(53) Konermann, L. *J. Phys. Chem. B* **2007**, *111*, 6534–6543.
(54) Iyengar, S. S.; Day, T. J. F.; Voth, G. A. *Int. J. Mass Spectrom.* **2005**, *241*, 197–204.
(55) Caleman, C.; van der Spoel, D. *Phys. Chem. Chem. Phys.* **2007**, *9*, 5105–5111.
(56) Berendsen, H. J. C.; Grigera, J. R.; Straatsma, T. P. *J. Phys. Chem.* **1987**, *91*, 6269–6271.
(57) Park, M.; Shin, I.; Singh, N. J.; Kim, K. S. *J. Phys. Chem. A* **2007**, *111*, 10692–10702.
(58) Cukierman, S. *Biochim. Biophys. Acta* **2006**, *1757*, 876–885.
(59) Marx, D. *ChemPhysChem* **2006**, *7*, 1848–1870.

intriguing effect adds a new perspective to the ongoing debate regarding the validity of the surface charge paradigm.

Methods

MD simulations were carried out based on C++ code developed in-house.[44] The temporal evolution of droplets consisting of 1248 SPC/E water molecules[56] in a vacuum environment was determined by integrating the classical equations of motion by use of the Verlet algorithm[60,61] with a time step of 2 fs. The water geometry is defined by a O−H bond distance of 1.0 Å and a H−O−H angle of 109.47°.[56] The system was initially subjected to Nose−Hoover thermalization[62,63] at 320 K for 80 ps. The simulation was then switched to constant-energy MD (at $T \approx 320$ K) for typically 1 ns, during which particle coordinates were extracted every 0.4 ps for analysis. Lennard-Jones (LJ) parameters for water were $\sigma_{OO} = 3.166$ Å and $\varepsilon_{OO} = 0.6502$ kJ mol^{-1}, with charges $q_O = -0.8476$e and $q_H = 0.4238$e.[56] Na^+ ions were modeled with $\sigma_{NaNa} = 2.586$ Å, $\varepsilon_{NaNa} = 0.4184$ kJ mol^{-1}, and $q_{Na} = +1.0$ e.[64] The mixing of LJ parameters for Na−O interactions was done according the Lorentz−Berthlot rules,[65] that is, $\sigma_{ij} = {}^1/_2(\sigma_{ii} + \sigma_{jj})$ and $\varepsilon_{ij} = (\varepsilon_{ii}\varepsilon_{jj})^{1/2}$, resulting in $\sigma_{NaO} = 2.876$ Å and $\varepsilon_{NaO} = 0.5216$ kJ mol^{-1}. Interactions between ions and SPC/E hydrogens were modeled purely on the basis of the Coulomb potential. LJ potentials were truncated at 9.5 Å but no cutoffs were used for Coulomb interactions. Electronic polarization effects were not considered in this work. Radial distributions represent histograms that are plotted versus the distance r from the droplet center of mass, corrected for the $4\pi r^2$ surface area of individual bins to account for the spherical geometry. Nanodroplet simulations were run on SHARCNET. Desktop computers were used for smaller test systems and code development. Images of MD frames were rendered by use of VMD.[66]

Results and Discussion

Conducting Sphere with Excess Charge. For the following discussion, it is helpful to briefly review the classical arguments[31] that provide the basis for the widely accepted surface charge paradigm of electrosprayed droplets.[5,24,25,27−30] For this purpose, we initially model a droplet as a solid sphere with radius R that consists of a homogeneous and electrically conducting material. The system accommodates a large number of charge carriers, resulting in an excess charge Q. At this level of description, the "ESI droplet" is treated analogously to a charged metal conductor. Gauss' law[31] states that the electric flux through any closed surface S is equal to the net charge q enclosed within this surface, divided by ε_0:

$$\oint_S \vec{E}\, d\vec{A} = \frac{q}{\varepsilon_0} \qquad (2)$$

$\vec{E}$ in this expression is the electric field, and $d\vec{A}$ is an infinitesimal surface element with a vector direction that coincides with the outward normal. We now evaluate the integral in eq 2 for a Gaussian surface that lies just inside the actual surface of the conductor, that is, where S encompasses all points with radial position $r = R - \delta$, with $\delta \ll R$. The key point for the argument made here is that the electric field $\vec{E}_{internal}$ anywhere inside a conductor has to be zero under equilibrium conditions.[31] Hence, it follows from eq 2 that the overall charge enclosed by the Gaussian surface is $q = 0$. In other words, all of the charge Q must be located on the surface of the sphere, at $r = R$.

Let us now assume that all charge carriers that constitute Q can be immobilized once equilibrium has been reached. In this way it is possible to map the Coulomb potential of the sphere by means of a point charge q_{test} without disturbing the existing charge distribution. The potential energy $V(r)$ of this point charge as a function of distance r from the droplet center is given by[31]

$$\begin{aligned} V(r) &= \text{constant} = CR^{-1} \quad \text{for } r \le R \\ V(r) &= Cr^{-1} \quad \text{for } r > R \end{aligned} \qquad (3)$$

with $C = Qq_{test}/(4\pi\varepsilon_0)$. Equation 3 represents the hallmark of *any* physical system where an overall charge Q is arranged in a thin spherical layer of radius R. This last point may appear trivial, but it will become important later on.

The behavior predicted by eq 2 is readily confirmed by simple MD simulations on charge carriers that are trapped within a spherical conductor of radius R. Figure 1 depicts a scenario where the interior of a sphere is modeled as vacuum, where Na^+ ions (mass = 23 Da) move with zero friction while experiencing only their mutual Coulomb repulsion. The boundaries of the conductor were defined by a radial trapping potential $V_{trap}(r) = kr$, with $k = 2000$ kJ mol^{-1} Å^{-1} for $r \ge R$, whereas $V_{trap}(r) = 0$ for $r < R$. The radius $R = 21$ Å chosen for this demonstration is typical for droplets during the final stages of the ESI process.[5]

Placing 500 ions within the sphere after thermalization at $T = 100$ K results in a spatial distribution where all charge carriers are spread across the surface. No ions are found in the interior (Figure 1A). The potential energy $V(r)$ of the sphere was mapped by using a point charge ($q_{test} = +e$), employing the strategy outlined above. Consistent with eq 3, this procedure reveals that $V(r)$ in the interior of the sphere is constant ($\vec{E}_{internal} = 0$). For $r > R$, $V(r)$ shows the expected r^{-1} dependence (Figure 1B).[31]

A very similar behavior with all charge carriers at the surface of the sphere is observed when the number of ions is reduced from 500 to 10 (Figure 1C, D). Close inspection of the $V(r)$ profile in Figure 1D reveals slight deviations from the ideal $\vec{E}_{internal} = 0$ behavior because charge can no longer be treated as a quasi-continuous entity. Raising the temperature to 1000 K leads to thermal broadening of the distributions in Figure 1A,C, but all ions remain confined to the outermost 1.5 Å (data not shown).

In summary, the data of Figure 1 confirm the surface charge paradigm[5,24,25,27−30] for an ideal conductor, even in cases where only relatively few ions are involved such that excess charge can no longer be treated as a quasi-continuum entity. Of particular interest for our discussion is Figure 1C,D, because the size and charge regime of that scenario is typical for droplets during the final stages of the ESI process. Specifically, an aqueous droplet with $R = 21$ Å and $\gamma = 0.072$ N m^{-1} that carries 10 elementary charges e is close to the Rayleigh limit ($Q = 0.83Q_R$, eq 1). The first scenario considered above exceeds the Rayleigh limit and was included for illustrative purposes only. On the basis of a two-dimensional model, it has previously been proposed that excess charges might be able to adopt stable positions in the interior of a conducting sphere.[50] Along with the predictions of eq 2, the results of Figure 1 reveal that for the three-dimensional case considered here such an assertion is not correct.

(60) Verlet, L. *Phys. Rev.* **1967**, *159*, 98–103.
(61) Frenkel, D.; Smit, B. *Understanding Molecular Simulations: From Algorithms To Applications*; Academic Press: San Diego, CA, 1996.
(62) Nose, S. *Mol. Phys.* **1984**, *52*, 255–268.
(63) Hoover, W. G. *Phys. Rev. A* **1985**, *31*, 1695–1697.
(64) Koneshan, S.; Rasaiah, J. C.; Lynden-Bell, R. M.; Lee, S. H. *J. Phys. Chem. B* **1998**, *102*, 4193–4204.
(65) Delhommelle, J.; Millie, P. *Mol. Phys.* **2001**, *99*, 619–625.
(66) Humphrey, W.; Dalke, A.; Schulten, K. *J. Mol. Graphics* **1996**, *14*, 33–38.

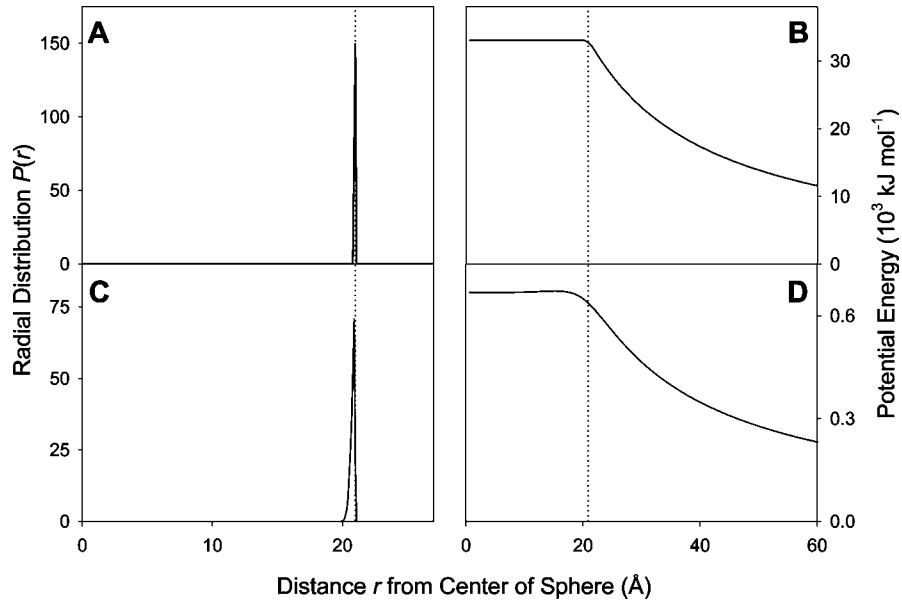

Figure 1. Results of constant-energy MD simulations for Na^+ ions that are trapped inside a hollow vacuum sphere at 100 K. Radial distributions are shown for the case of (A) 500 and (C) 10 ions. Panels B and D show the corresponding potential energy profiles, obtained by immobilizing the ion positions and mapping the Coulomb energy of a point charge ($+e$) as a function of radial distance r from the center of the sphere. To avoid singularities during this mapping procedure, the Coulomb potential was truncated for charge−charge distances of less than 1 Å. Dotted lines at $r = 21$ Å indicate the radius of the sphere.

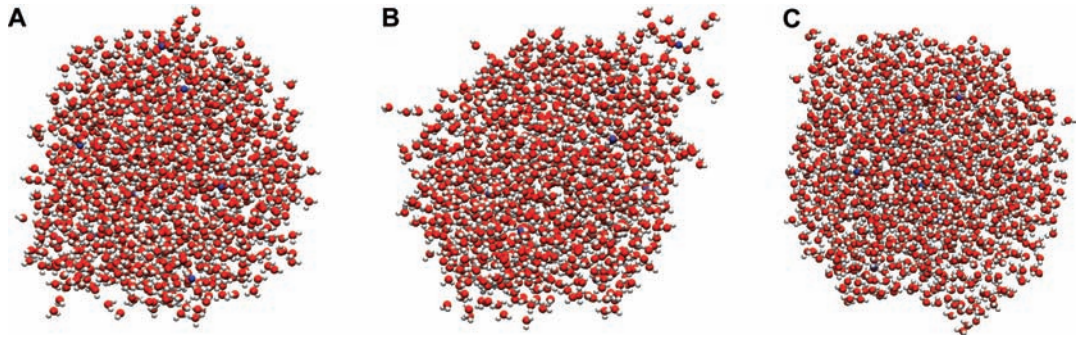

Figure 2. Snapshots taken from MD simulations of SPC/E water nanodroplets (O, red; H, white) containing 1248 H_2O and 10 charge carriers (blue). Panels A and B are for a system containing Na^+, whereas panel C is for a droplet that contains X^- (see text for details).

Water Droplets Carrying Na^+ and X^- Ions. We will now depart from models that treat ESI nanodroplets as unstructured conductors and instead explore the behavior of aqueous systems containing atomic ions. The droplets considered here have radii of around 21 Å, comparable to the examples of Figure 1. MD simulations on these aqueous systems were based on the full set of LJ and Coulomb potentials, as described in the Methods section. In addition to exploring the behavior of systems with 10 Na^+ ions that are close to the Rayleigh limit, we also consider water droplets that contain only a single ion. Additionally, we examine the behavior of negatively charged ($-e$) ions having the same mass and LJ characteristics as Na^+. Although these so-called "X^- ions" do not correspond to any naturally occurring species, they represent a useful tool for comparative studies that provide insights into the origin of Na^+ behavior.[36]

Water droplets containing 10 Na^+ maintain a shape that is roughly spherical during most of the 1 ns simulation window (Figure 2A). Evaporation is negligible on this time scale at the temperature used (320 K), but the droplets undergo occasional surface undulations (Figure 2B). Droplets containing 10 X^- exhibit a similar behavior (Figure 2C). These observations are consistent with earlier MD studies.[15,44,50−52]

The most pertinent issue in the context of the current study is the location of ions within these aqueous systems. In stark contrast to the behavior seen for an unstructured conducting sphere (Figure 1), excess Na^+ and X^- ions are *not* located on the surface of the aqueous droplets. This is illustrated in Figure 3, where ionic radial distributions are depicted together with those of H and O. For all cases considered here the water density in the interior is approximately constant, followed by a sigmoidal transition region toward the vapor phase with a midpoint of roughly 21 Å. Droplets carrying 10 Na^+ exhibit a broad ion distribution centered at 13 Å (Figure 3A). For systems carrying only one Na^+, the charge distribution is more narrow and its centroid is shifted to $r = 9.4$ Å (Figure 3B). The charge distribution for 10 X^- is similar to that observed in the case of 10 Na^+, with a centroid at 13 Å (Figure 3C). Droplets carrying single X^- exhibit a distribution with a centroid at 14 Å (Figure 3D). The general phenomena depicted in Figure 3 are in line with earlier simulation studies.[50,52,55] In the following sections we will explore the internal droplet structure in more detail, with the aim of uncovering why the observed ion distributions are in apparent violation of the surface charge paradigm.[5,24,25,27−30]

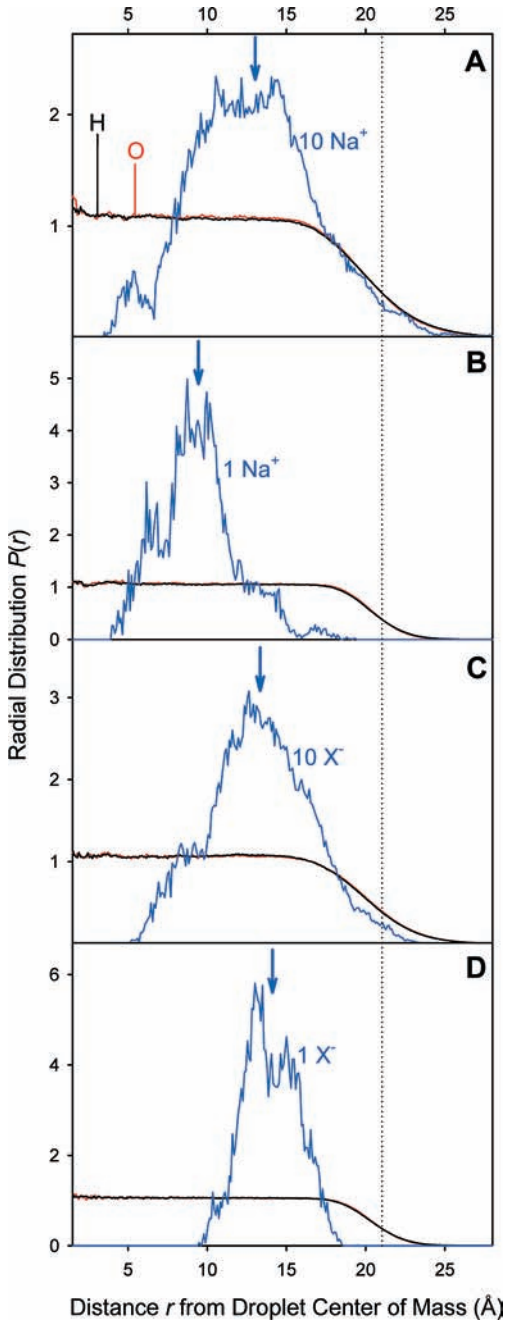

Figure 3. Radial distributions of charge carriers (blue) in aqueous droplets containing (A) 10 Na^+, (B) one Na^+, (C) 10 X^-, and (D) one X^-. Vertical blue arrows represent the centroids of these ion distributions. Water distributions are included for comparison (oxygen, red; hydrogen, black). Data were averaged over three 1 ns runs for each panel. The dotted line at $r = 21$ Å indicates the approximate position of the liquid/vapor interface.

Local Ion Solvation. For droplets carrying 10 sodium ions, the O/Na^+ pair correlation function exhibits a dominant maximum at 2.5 Å and a smaller, more diffuse peak at 4.5 Å. The corresponding H/Na^+ signals are found at 3.1 and 5.2 Å (Figure 4A). These double peaks for oxygen and hydrogen represent the first and second solvation shells of Na^+. A typical first solvation shell structure is displayed in the inset of Figure 4A, showing Na^+ with its six nearest-neighbor water molecules in an approximately octahedral arrangement where the oxygens point toward the ion. A dramatically different solvation pattern is observed for X^- (Figure 4B). While still being surrounded

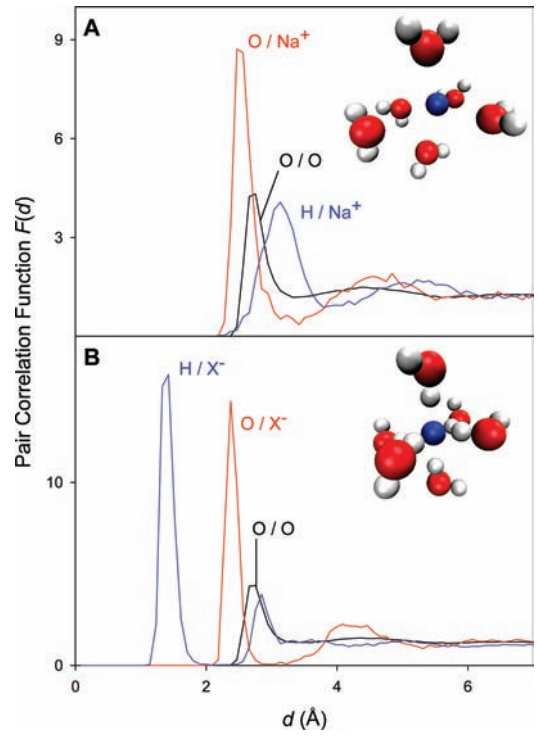

Figure 4. Local solvation patterns of (A) Na^+ and (B) X^-, as revealed through pair correlation functions with oxygen and hydrogen. Oxygen−oxygen data are included for comparison. Insets depict typical snapshots of (A) Na^+ and (B) X^- first solvation shells, obtained by selecting all waters contained within a 3.5 Å sphere around the ion. The data depicted here were obtained for droplets with 10 ions; very similar results (not shown) were obtained for systems containing a single ion.

by six waters, these ions are in close contact with hydrogens, while the oxygen atoms tend to point away from the charge center.[67] These differences are readily apparent from the pair correlation function in Figure 4B, which has its main H/X^- maximum at 1.4 Å and a smaller peak at 2.8 Å. The corresponding O/X^- maxima are at 2.4 and around 4.2 Å. The relative orientations of water molecules in the second solvation shell are similar to those of the first shell, albeit the former are more disordered (data not shown). The local solvation phenomena depicted in Figure 4 are consistent with neutron and X-ray scattering, as well as modeling data obtained for ions in bulk solution.[64,68,69]

Macrosolvation. Orientational preferences of water can be analyzed by considering the angle θ between the H_2O dipole moment (H−O−H bisector) and the vector that points from oxygen to the droplet center of mass (Figure 5). For this analysis the droplets are divided into radial shells with a thickness of 5 Å. We will first examine the dipole orientations for purely aqueous systems, that is, in the absence of ions. The $P(\cos\theta)$[70−72] distributions in this case are flat for radial shells up to approximately 15 Å from the center, representing bulklike water molecules in random orientations (Figure 5A). Orientational

(67) Tielrooij, K. J.; Garcia-Araez, N.; Bonn, M.; Bakker, H. J. *Science* **2010**, *328*, 1006–1009.
(68) Bouazizi, S.; Nasr, S.; Jaidane, N.; Bellissent-Funel, M.-C. *J. Phys. Chem. B* **2006**, *110*, 23515–23523.
(69) Marcus, Y. *Chem. Rev.* **2009**, *109*, 1346–1370.
(70) Brodskaya, E. N.; Eriksson, J. C.; Laaksonen, A.; Rusanov, A. I. *J. Colloid Interface Sci.* **1996**, *180*, 86–97.
(71) Rossky, P. J.; Karplus, M. *J. Am. Chem. Soc.* **1979**, *101*, 1913–1937.
(72) Belch, A. C.; Berkowitz, M. *Chem. Phys. Lett.* **1985**, *113*, 278–282.

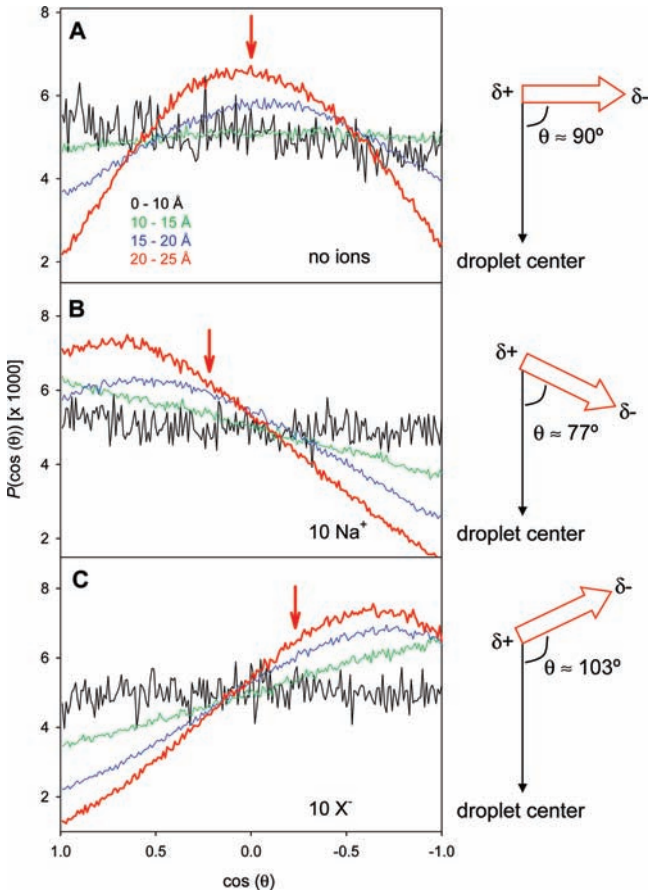

Figure 5. Distribution functions of the angle θ between the water dipole vector and the vector pointing from oxygen to the droplet center. The panels are for (A) droplets without ions, (B) droplets with 10 Na^+, and (C) droplets with 10 X^-. Data are shown for four different droplet radial shells: 0−10 Å (black), 10−15 Å (green), 15−20 Å (blue), and 20−25 Å (red). Vertical red arrows represent centroids of the 20−25 Å (red) distributions. Schematic diagrams along the right-hand side depict the most likely water dipole orientations in the 20−25 Å radial shell for each of the three cases.

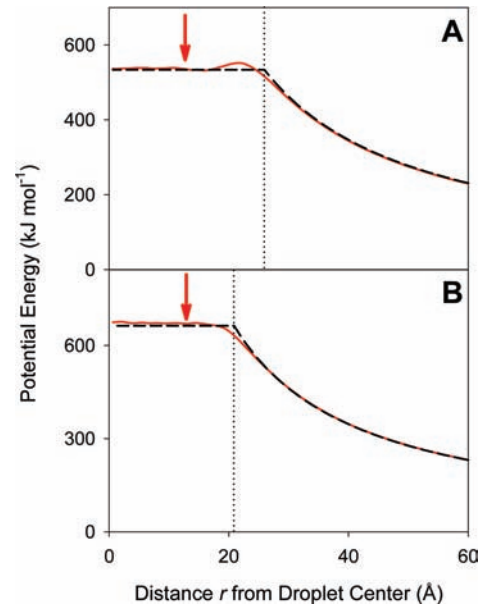

Figure 6. (A) Red curve: Coulomb energy profile experienced by a point charge ($q_{test} = +e$) for droplets containing 10 Na^+ ions. This profile includes all interaction of the point charge with H, O, and Na^+. Dashed line: $V(r)$ profile predicted by eq 3 for a sphere that carries a surface charge layer of $Q = +10e$ at $R = 26$ Å. (B) Same as in panel A but for droplets containing 10 X^- ions and a point charge $q_{test} = -e$. The theoretical $V(r)$ profile in panel B is based on $Q = -10e$ and $R = 21$ Å. Red vertical arrows denote centroids of ion radial distributions from Figure 3A,C. Vertical dotted lines indicate R values. Red profiles represent data that were averaged over three 1 ns MD runs.

preferences become increasingly apparent for radial shells toward the droplet surface. The outermost layer considered here (20−25 Å, red in Figure 5A) exhibits a maximum at cos $\theta \approx 0$, corresponding to a preferred orientation where the water dipole moments lay flat on the droplet surface ($\theta \approx 90°$). This finding is consistent with earlier work.[72−76] Surface ordering is further enhanced for layers that are even farther removed from the droplet center ($r > 25$ Å),[44] but those data are not included in Figure 5 due to the low particle density in those regions (see Figure 3). Angular distributions for systems carrying single Na^+ or X^- ions (not shown) are very similar to those of pure water in Figure 5A.

Dramatically different dipole orientations are observed for systems that contain 10 excess ions. In the case of droplets with 10 Na^+, water close to the surface exhibits preferred orientations where the negative (oxygen) end of the dipole moment is tilted toward the droplet interior at an angle of $\theta \approx 77°$ (Figure 5B). The opposite effect is observed for droplets with 10 X^- ions, resulting in preferred surface orientations where oxygen points away from the interior at $\theta \approx 103°$ (Figure 5C). The data of Figure 5 demonstrate that the presence of 10 excess ions has profound consequences for all molecules located within the outer droplet layers. The sign of the excess charge electrostatically dictates the tilt angle of the water dipoles. The resulting large-scale orientational polarization provides enthalpically favorable charge−dipole interactions that go far beyond the local solvation patterns depicted in Figure 4. [Readers are reminded that *electronic polarization* refers to the induction of dipole moments in an electric field, an effect that is not considered in our study (see Introduction). In contrast, *orientational polarization* results from the alignment of pre-existing dipole moments. The latter phenomenon is fully captured by the modeling strategy used here.]

Location of Charge in Droplets with Excess Ions. We will now return to the key question addressed in this work, namely, the ion distribution within highly charged water nanodroplets. As pointed out, our finding that Na^+ and X^- reside in the interior (Figure 3) is in apparent conflict with the general notion[5,24,25,27−30] that excess charge carriers should be located on the droplet surface.

The key to solving this conundrum is found by mapping the Coulomb energy of a point charge ($q_{test} = +e$) that probes the combined contributions of all H, O, and Na^+ charge centers within the droplet. Remarkably, the time-averaged energy profile for droplets containing 10 Na^+ is virtually constant up to $r \approx 26$ Å, followed by a r^{-1} decrease (red curve in Figure 6A). Superimposed on these data is the $V(r)$ profile of an arrangement where a charge of $Q = +10e$ is evenly spread on the surface of a sphere with $R = 26$ Å (eq 3, dashed line in Figure 6A). It is evident that the two profiles are in very close agreement with each other. On the basis of the discussion above (eq 3), we

(73) Wang, L.; Hermans, J. *Mol. Simulat.* **1996**, *17*, 67–74.
(74) Townsend, R. M.; Rice, S. A. *J. Chem. Phys.* **1991**, *94*, 2207–2218.
(75) Lee, C.-Y.; McCammon, J. A.; Rossky, P. J. *J. Chem. Phys.* **1984**, *80*, 4448–4455.
(76) Kathmann, S. M.; Kuo, I.-F. W.; Mundy, C. J. *J. Am. Chem. Soc.* **2008**, *130*, 16556–16561.

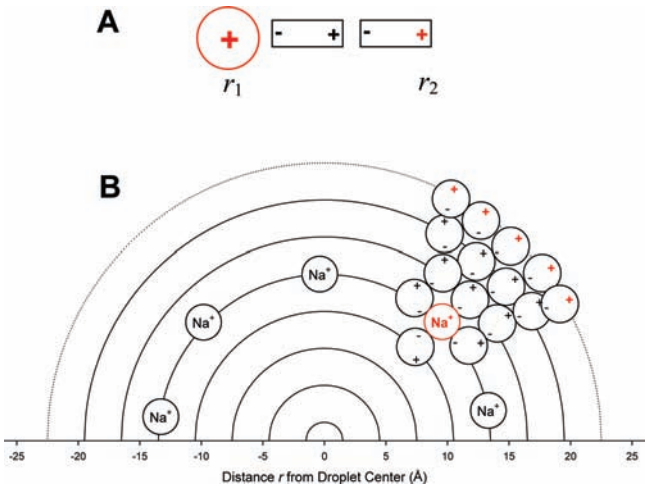

Figure 7. (A) Schematic cartoon, illustrating how the interaction of a cation with two oriented dipoles effectively transfers a fraction of the positive charge from position r_1 to r_2. (B) Schematic semicross-section through an aqueous nanodroplet carrying excess Na^+ ions. Concentric circles represent the approximate spacing of water molecules. For one of the Na^+ ions (red), this cartoon illustrates how orientational polarization of water dipoles acts to transfer the ionic charge from the interior to the surface. Note that this representation greatly exaggerates the extent of water ordering, compared to the actual situation of Figure 5.

have to conclude that droplets containing 10 Na^+ carry all their excess charge in a surface layer located ca. 26 Å from the droplet center.

How is it possible for excess charge to reside at the extreme periphery of the droplet ($r \approx 26$ Å), while all 10 Na^+ are buried in the interior ($r \approx 13$ Å)? Figure 7A shows in cartoon representation how the interaction of an ion with two oriented dipoles effectively neutralizes a fraction of the ionic charge at site r_1, thereby transferring this fractional charge to the opposite end of the dipole chain at r_2. In Figure 7B it is illustrated how the large-scale orientational polarization of water molecules (Figure 5B) leads to charge transfer from buried Na^+ to the droplet surface via such a mechanism. Thus, Na^+ ions in the droplet interior become effectively "neutralized" by solvation, while the positive ends of water dipoles at the droplet periphery assume the role of surface charge.

A transfer mechanism symmetrical to that illustrated in Figure 7 for Na^+ is also operative for droplets containing 10 X^-. Following arguments that are analogous to those outlined above, Coulomb energy scanning with $q_{test} = -e$ reveals that excess charge is entirely located on the droplet surface, although the X^- ions reside in the interior (Figure 6B). In the case of X^-, the orientational solvent polarization (Figure 5C) causes the *negative* ends of the water dipoles at the droplet periphery to assume the role of surface charge. The location of the resulting surface charge layer is at $r \approx 21$ Å (Figure 6B).

The discussion of this paragraph reconciles the surface charge paradigm for ESI nanodroplets[5,24,25,27–30] with the tendency of small atomic ions to maximize enthalpically favorable solvation by migrating into the interior. Excess charge is indeed located on the droplet surface, but only in the form of half-dipoles that point into the water–vapor interface as a result of orientational solvent polarization. This arrangement allows all ions to remain fully solvated in the droplet interior. In contrast to earlier proposals,[25,50] therefore, the presence of a charged surface layer on ESI nanodroplets does *not* imply that the actual charge carriers (ions) have to be located at the water/vapor interface.

The charge transfer phenomenon illustrated in Figure 7 bears a remote analogy to the Grotthus mechanism of H^+ transfer in water,[58,59] but we caution that this comparison should not be overextended. Grotthus migration involves the rearrangement of H-bonds, whereas the effect considered here originates from the orientation of pre-existing dipoles.

Preferred Ion Depth. The previous discussion has made it clear that Na^+ and X^- do not reside at the droplet surface because this would imply the loss of enthalpically favorable local solvation, as well as macrosolvation. On the other hand, Figure 3 reveals that the ions also avoid the innermost droplet regions, giving rise to preferred positions in the 9–14 Å range. It is interesting to briefly discuss the factors that determine the optimal penetration depth of the ions relative to the droplet center.

In the absence of any other considerations, one might naively assume that ion solvation is most favorable at $r \approx 0$. For droplets containing multiple ions it is obvious, however, that positions in the droplet center will be disfavored by mutual Coulomb repulsion as well as solvation shell distortions (Figure 4). The significance of both aspects can be tested by reducing the number of ions from 10 to one, such that charge–charge repulsion and the distortion of solvation shells by other ions are eliminated.

Consistent with our expectation, droplets containing a single Na^+ have their centroid shifted somewhat more to the droplet center than the systems containing 10 Na^+ (Figure 3A,B). However, in the case of X^- this effect is not observed (Figure 3C,D). More importantly, even for the single ion systems there remains an obvious tendency to avoid the innermost regions (Figure 3B,D). We conclude that ion exclusion from the $r \approx 0$ region must involve factors in addition to those considered above. Specifically, we note that any ordering of water is entropically unfavorable.[46] The droplet interior ($r < 10$ Å) has bulklike properties without any orientational preferences for all the systems studied here (Figure 5). Placing an ion with its relatively ordered local solvation shells (Figure 4) close to the center would reduce the entropy of the droplet interior, thereby repelling ions from the center region. We propose that this "entropic buoyancy" is a major factor that prevents ions from venturing close to the droplet midpoint.

Conclusions

This study examined the structure of aqueous nanodroplets containing excess charge due to the presence of small atomic ions. Droplets of this type play an important role for mechanistic studies on the ESI process.[5,15,25,50,77] Understanding the physical properties of these systems, therefore, is of considerable importance.

The widely accepted notion that excess charge is located on the surface of ESI nanodroplets is in apparent conflict with the well-known tendency of ions such as Na^+ to maximize charge–solvent interactions by migrating toward the bulk. The MD simulations of this work confirm that charged droplets exhibit ion radial distributions centered around $^2/_3R$ (for $R \approx 21$ Å), where solvation requirements are fully satisfied. In other words, *excess Na^+ ions are not located at the droplet surface*. Nonetheless, Coulomb energy mapping reveals that *all excess charge is confined to a thin layer at the droplet periphery*. These

(77) Van Berkel, G. J.; De La Mora, J. F.; Enke, C. G.; Cole, R. B.; Martinez-Sanchez, M.; Fenn, J. B. *J. Mass Spectrom.* **2000**, *35*, 939–952.

seemingly contradictory findings are reconciled on the basis of charge-induced orientation of water dipole moments. Ions in the droplet interior become effectively neutralized through charge−dipole interactions. Orientational polarization of water molecules then acts to transfer the excess charge to the droplet periphery. Figure 7 illustrates how the charge layer generated in this way at the water/vapor interface can be thought of as unpaired half-dipoles. This layer has exactly the same time-averaged magnitude as the buried ionic charge Q (Figure 6). Related phenomena have recently been discussed by Consta.[78]

Although not explicitly addressed in this work, our findings have implications for the mechanism by which Na^+ and other small ions are released into the gas phase during the final stages of ESI. It is usually assumed that this process occurs via the ion evaporation mechanism.[5,25,26] According to this model, ions reside close to the surface of the droplet, from where they can be electrostatically ejected. Our results indicate that excess Na^+ ions are not part of the charged surface layer, such that their ejection directly from the water/vapor interface may not be feasible. Recent work suggests that these emission events more likely proceed through thin liquid jets.[15] In future work it will be interesting to extend studies of the type performed here to aqueous/organic solvent mixtures and other ESI charge carriers, including hydrated protons and ammonium ions.

Acknowledgment. We thank Professor Martin H. Müser for stimulating discussions and critical reading of the manuscript. This work was financially supported by the Natural Sciences and Engineering Research Council of Canada (NSERC), The University of Western Ontario, and the Canada Research Chairs Program. Simulations were carried out at the SHARCNET facility (www.sharcnet.ca).

JA1041989

(78) Consta, S. *J. Phys. Chem. B* **2010**, *114*, 5263–5268.